Density Waves and Cooper Pairing on the Honeycomb Lattice

Carsten Honerkamp

Theoretical Physics, Universität Würzburg, D-97074 Würzburg, Germany

(Received 16 November 2007; published 11 April 2008)

Motivated by the surge in research activities on graphene, we investigate instabilities of electrons on the honeycomb lattice, interacting by onsite and nearest-neighbor terms, using a renormalization group scheme. Near half band filling, critical minimal interaction strengths are required for instabilities toward antiferromagnetic or charge-density-wave order. Away from half-filling, f-wave triplet-pairing and $d + id$ singlet-pairing instabilities are found to emerge out of density-wave regimes.

DOI: 10.1103/PhysRevLett.100.146404 PACS numbers: 71.10.Fd, 74.20.Mn, 74.70.Wz

Recently it has become possible to fabricate graphene [1]. Already its structure poses some interesting questions to experiment and theory [2]. The massless-Dirac spectrum near the two Fermi points of the undoped system gives rise to novel quantum Hall effects and many more complex physical puzzles [2]. Mesoscopic properties of graphene as specular Andreev reflection [3], analogues to relativistic quantum mechanics [4] or spin quantum bits with graphene [5] are discussed intensively.

Obviously, the question arises if graphene features any interesting many-body states. Until now, no drastic anomalies have been reported [6]. Superconductivity in graphite compounds is usually attributed to extrinsic causes, e.g., to interlayer states for intercalated compounds [7] or, more intriguing and less clear-cut, to disorder of sulfur atoms in graphite-sulfur composites [8]. Intrinsic pairing in 2D graphene would be a fascinating finding. In theory, the electronic self-energy for undoped graphene is of marginal Fermi liquid type [9]. Upon doping a normal Fermi liquid develops [10]. The Dirac spectrum should further be reflected in the dependence of the phonon renormalization on the electron density [11].

There have been various theoretical studies of ordered states on the honeycomb lattice [12–18] driven by interactions, but to date no comprehensive picture for a wider range of interaction parameters and band fillings is available. Here we investigate intrinsic interaction effects on the honeycomb lattice for a range of short-ranged interactions and dopings, using the perturbative functional renormalization group (FRG). This method works in the thermodynamic limit and goes beyond the $1/N$- or mean-field-approximations of Refs. [13,15,17]. It is well suited to treat competing orders as it includes the coupling of collective fluctuations in an unbiased way. Recently it has been applied to two-dimensional (2D) Hubbard models on square [19–22] and triangular lattices [23,24].

Our model is a 2D honeycomb lattice with nearest-neighbor hopping amplitude t. The interaction terms contain onsite and nearest-neighbor repulsions U and V, and a spin-spin interaction J. The restriction to short-range terms is partly due to the difficulty to treat a long-range Coulomb part directly in the FRG approach. However, most experimental graphene systems are doped to some degree. Hence at least the effective interaction is screened, and our starting point may not be unrealistic. Furthermore, for the undoped case, the long-range part was shown [15] to be marginally irrelevant in $1/N$; hence, our results for short-range interactions may even be useful in the undoped case. The Hamiltonian reads

$$H = -t \sum_{\langle i,j\rangle,s} (c^\dagger_{i,s} c_{j,s} + c^\dagger_{j,s} c_{i,s}) + U \sum_i n_{i,\uparrow} n_{i,\downarrow} + V \sum_{\langle i,j\rangle,s,s'} n_{i,s} n_{j,s'} + J \sum_{\langle i,j\rangle} \vec{S}_i \cdot \vec{S}_j. \quad (1)$$

$\langle i, j\rangle$ denotes all pairs of neighbored sites and $\vec{S}_i = \frac{1}{2} \sum_{ss'} c^\dagger_{i,s} \vec{\sigma}_{ss'} c_{i,s'}$.

The FRG scheme used here is an approximation to an exact flow equation for the one-particle irreducible vertex functions of a many-fermion system when a parameter in the quadratic part of the action is varied [25]. In the temperature-flow scheme employed here, the temperature T is used as flow parameter. The FRG flow is generated by lowering T from an initial value T_0 where the perturbative corrections are negligible. In the approximation we use for the flow [22], the derivative of the interaction vertex V_T with respect to T is given by the T derivative of one-loop corrections. These one-loop diagrams are of second order in the vertices V_T and include particle-hole diagrams, e.g., vertex corrections and screening, and particle-particle diagrams. Higher loop contributions are generated by the integration of the flow. Like in many previous works using this method, the self-energy feedback on the flow of V_T is neglected. It may become important when the interactions get large. Hence the flow is stopped when the interaction strength exceeds twice the bandwidth. The method is controlled in the limit of small interactions. For the interesting case of moderate interactions, it should be viewed as a step beyond the meanfield level that captures the evolution and competition of various correlations in an unbiased way.

The interaction vertex can be expressed by a coupling function $V_T(k_1, k_2, k_3)$. It depends on the generalized wave vectors of two incoming particles (k_1 and k_2) and one outgoing (k_3) particle with wave vector, Matsubara fre-

quency, and spin projection $k_i = (\vec{k}_i, \omega_i, s_i)$. In the search for instabilities toward symmetry breaking, the frequency dependence is neglected and the ω_i are set to zero. The $\vec{k}$ dependence of remaining function $V_T(\vec{k}_1, \vec{k}_2, \vec{k}_3)$ is discretized in the so-called N-patch scheme, introduced in this context in Ref. [19]. For cases with a FS, this amounts to keeping $V_T(\vec{k}_1, \vec{k}_2, \vec{k}_3)$ constant within patches labeled by $k_i = 1, \ldots, N$ perpendicular to the FS. This defines an N^3 component coupling function $V_T(k_1, k_2, k_3)$, which is computed for $\vec{k}(k_i) = \vec{k}_i$, $i = 1, \ldots, 3$, on the FS. As for the honeycomb lattice there is no FS at half band filling, we generalize the patching scheme to two or three rings of 18 or 24 patches around the Dirac points (see Fig. 1). In addition, $V_T(k_1, k_2, k_3)$ depends on 4 band or sublattice indices for the 2 incoming and 2 outgoing particles. For brevity, these indices are not shown in our notation, but mentioned if necessary.

The RG flow is started at an initial temperature T_0. The initial interaction is given by the bare interaction with the onsite repulsion U and the nearest-neighbor interactions V and J. Specifically, we search for *flows to strong coupling*, where for a certain low temperature T_c one or several components of $V_T(k_1, k_2, k_3)$ become large. At this point the approximations break down, and the flow has to be stopped. Information on the low-T state is obtained by analyzing which coupling functions grow most strongly and from the flow of susceptibilities. In particular for 2D systems, this instability does not guarantee true long-range order. Rather, it should be interpreted as a breakdown of the (semi-)metallic state and as indicator for the leading correlations at low T.

Beginning with the semimetal for chemical potential $\mu = 0$, we first find perturbative stability. Starting the RG at high T and small U, V or J, we can follow the flow down to lowest T without a divergence. This is different from systems with a finite density of states at the Fermi energy, where the flow practically always leads to some kind of instability. In our case, the absence of a flow to strong coupling indicates the absence of long-range order due to electronic interactions even at lowest T.

Next we increase the bare interactions. Above a critical value $U_c \sim 3.8t$ for the onsite repulsion U with $V = J = 0$, the interactions flow to strong coupling. The static antiferromagnetic (AF) spin susceptibility grows most strongly toward the critical temperature scale, indicating a tendency toward AF spin-density-wave (SDW) formation with opposite orientation of the ordered spin moment on A and B sublattices. For small U, $J = 0$, and increasing nearest-neighbor repulsion V we again find a flow to strong coupling for $V > V_c \sim 1.2t$, now with leading charge-density-wave (CDW) correlations for different charge densities on the two sublattices. This compares favorably with a previous $1/N$ analysis [15] finding the same instabilities beyond critical values U_c and V_c. There is also good agreement with the early Quantum Monte Carlo work by Sorella [12] who found a transition to an AF Mott-state at $U \sim 4t$. In Fig. 1 we show the dependence of the critical temperature T_c for the flow to strong coupling vs U and V. The critical U of the SDW instability is more or less unaffected by an increasing V, while V_c for the CDW regime is shifts to larger V with a roughly linear dependence on U. When the two lines meet, there is a continuous change from leading SDW to leading CDW correlations (or vice versa). This is consistent with a first order transition, if order is possible at all. The competition for the spectral weight not included in this study as the self-energy

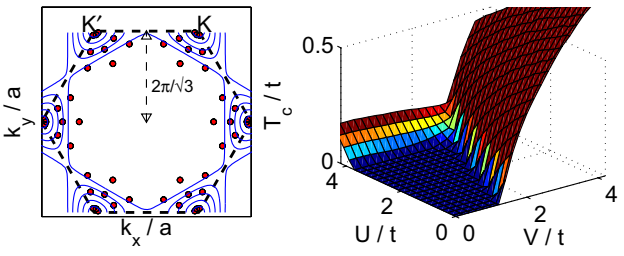

FIG. 1 (color online). Left: Brillouin zone and 18×3 points used for discretizing the wave-vector dependent interaction. The solid lines are at constant band energy. The lattice constant (minimal distance between 2 A-sublattice sites) is set to 1. Right: Critical temperature T_c for the flow to strong coupling vs interaction parameters U, V at half-filling $\mu = 0$, $J = 0$. In the region with $T_c = 0$, the semimetal is stable. For small U and $V > 1.2t$, the flow is toward a CDW instability, for small V and $U > 3.8t$ toward a SDW instability.

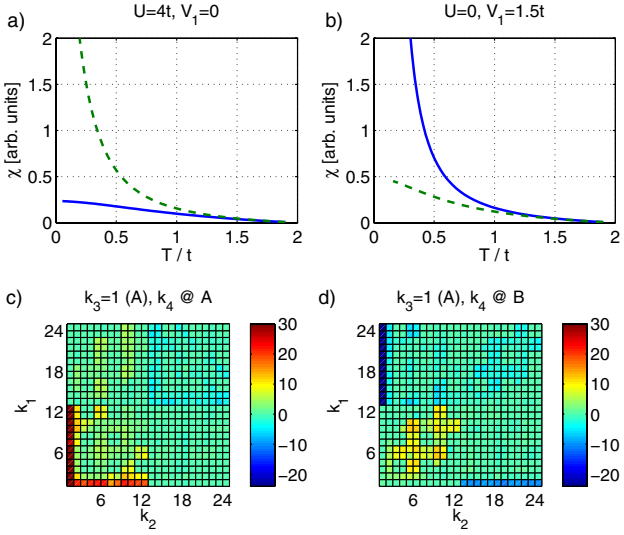

FIG. 2 (color online). Upper plots: Flow of susceptibilities, solid line CDW, dotted line SDW, for (a) $U = 4t$, $V = 0$, (b) $U = 0$, $V = 1.5t$. Lower plots: Interactions $V_T(k_1, k_2, k_3)$ very close to the SDW instability at $T_c \approx 0.05t$ for $U = 4t$, $V = 0$. The colorbar indicates the values of the couplings. The incoming wave vectors k_1 and k_2 are on the inner rings near the Dirac points, for $k_{1/2} = 1$ to 12 on sublattice A, and $k_{1/2} = 13$ to 24 for SL B. The 1st outgoing particle k_3 is at point 1 and SL A. In (c), the 2nd outgoing is on SL A, in (d) on SL B.

is neglected could, however, reduce the ordered moments in the transition region.

In Fig. 2 we display the flow of various susceptibilities for SDW and CDW instabilities, and V_T very close to T_c. The actual calculation takes place in the fermionic basis which diagonalizes the hopping term. The resulting interactions are transformed back into the sublattice (SL) basis with operators $c^{(\dagger)}_{\vec{k},s,l}$ on SL $l = A, B$ for incoming and outgoing particles. In Figs. 2(c) and 2(d) we show the real part of $V_T(k_1, k_2, k_3)$ close to T_c of the SDW instability, for the incoming wave vectors varying over 12 $\vec{k}$-space points labeled by k_1 and k_2 on the innermost rings around the Dirac points in the left plot of Fig. 1. The 12 points are numbered in a clockwise fashion around the Brillouin zone hexagon. Points 1,2 are near $\vec{K}$, points 3 and 4 near $\vec{K}'$, and so on. Points 1 to 12 refer to particles on SL A, points 13 to 24 are numbered in the same way for SL B. The first outgoing wave vector is fixed at point $k_3 = 1$ on SL A. $V_T(k_1, k_2, k_3)$ shows either vertical or horizontal features

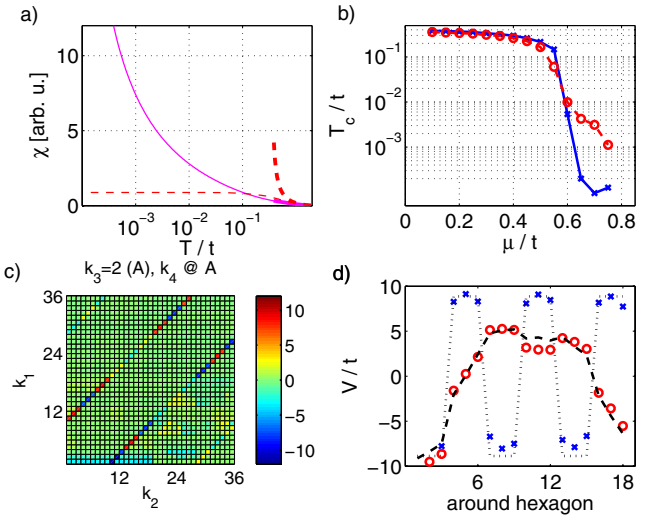

FIG. 3 (color online). (a) Flow of pairing susceptibilities in f-wave (solid lines) and CDW channel (dashed lines) for chemical potentials $\mu = 0.1t$ (thick lines) to $\mu = 0.75t$ (thin lines). (b) T_cs for the flow to strong coupling vs μ. Crosses: $U = 1.2t$, $V = 2.4t$ with a CDW instability for $\mu < 0.7t$ and a triplet Cooper instability for $\mu > 0.7t$. Circles: $U = 1.2t$, $J = 2.4t$ with a SDW instability for $\mu < 0.65t$ and a singlet d-wave Cooper instability for $\mu \geq 0.65t$. (c) Interaction at low scales for $U = 1.2t$, $V = 2.4t$, $\mu = 0.75t$, and outgoing wave vectors fixed on SL A, $k_3 = 2$ for a 18×3 discretization. Points k_1 and k_2 are on the middle of the three rings nearest to the FS and on SL A for index 1 to 18 and on B for 19 to 36. The color bar indicates the values of the couplings. (d) Crosses: Pair scattering $V_T(k_1, \bar{k}_1, k_2)$ for $U = 1.2t$, $V = 2.4t$, $\mu = 0.75t$ with incoming and outgoing particles on SL A and $\vec{k}_1 + \vec{k}(\bar{k}_1) = 0$ vs k_2 around the Brillouin zone hexagon. The dotted line is the ansatz $-V_f d^*_f(\vec{k}_1) d_f(\vec{k}_2)$. Circles: Same data for the d-wave instability at $U = 1.2t$, $J = 2.4t$, $\mu = 0.75t$. Here the dashed line is $-V_d[d^*_{x^2-y^2}(\vec{k}_1) d_{x^2-y^2}(\vec{k}_2) + d^*_{xy}(\vec{k}_1) d_{xy}(\vec{k}_2)]$.

with strongly attractive or repulsive values. The vertical features have $k_2 = k_3$ (i.e., same wave vector, same SL for particles 2 and 3) or $k_2 = k_3 \pm 12$ (same wave vector, but different SLs for particles 2 and 3). From these features the dominant instability can be read off, e.g., by comparing $V_T(k_1, k_2, k_3)$ to an infinite-range interaction which gives a SDW as ground state. On a lattice with N sites, we can define spin-spin interactions $N^{-1}\sum_{\vec{q}} J^{l,l'}_{\vec{q}} \vec{S}^l_{\vec{q}} \cdot \vec{S}^{l'}_{-\vec{q}}$ with $\vec{S}^l_{\vec{q}} = \frac{1}{2}\sum_{\vec{k}} \vec{\sigma}_{ss'} c^\dagger_{\vec{k}+\vec{q},s,l} c_{\vec{k},s',l}$. For the infinite-range SDW interaction, only the $\vec{q} = 0$ components in $J_{\vec{q},l,l'}$ are nonzero. We should have $J^{l,l}_{\vec{q}=0} < 0$, i.e., ferromagnetic (FM) on the same SL, while $J^{l,l'}_{\vec{q}=0} > 0$, i.e., AF, for different SLs $l \neq l'$. Comparing this with the effective interaction from the FRG,

$$\frac{1}{2N} \sum V^{l_1 l_2 l_3}_T(\vec{k}, \vec{k}', \vec{k} + \vec{q}) c^\dagger_{\vec{k}+\vec{q},s,l_3} c^\dagger_{\vec{k}'-\vec{q},s',l_4} c_{\vec{k}',s',l_2} c_{\vec{k},s,l_1},$$

we get $V^{ll'l'}_T(\vec{k}, \vec{k}', \vec{k}' - \vec{q}) = -J^{l,l'}_{\vec{q}}$ and $V^{ll'l}_T(\vec{k}, \vec{k}', \vec{k} + \vec{q}) = -J^{l,l'}_{\vec{q}}/2$. In the FRG data in Fig. 1(c) and 1(d), only the $\vec{q} = 0$ interactions grow strongly, and the signs depending on the SL follow exactly that of the reduced spin-spin-interaction with FM intra-SL and AF inter-SL processes. The CDW instability is read off from V_T in similar way.

Next we turn to the doped system. Specifically we search for density-wave driven Cooper pairing. $\mu \neq 0$ creates two FSs around the Dirac points. The $\vec{q} = 0$ nesting between the two bands is reduced. This cuts off the CDW and SDW instabilities at low T. The behavior of the CDW susceptibility and T_c vs μ is shown in Fig. 3(a) and 3(b). The SDW instability for dominant U (or J) behaves analogously. Beyond a critical doping, the CDW susceptibility remains finite for $T \to 0$. If we continue the flow down to lower temperatures $T < 10^{-3}t$, we observe a strong growth in the Cooper pairing processes with zero total incoming wave vector. This is clearly visible in the effective interactions near T_c shown in Fig. 3(c) for $\mu = 0.75t$. Here, processes with zero total incoming wave vector (diagonal features) are enhanced strongly. The pair scattering $V_T(\vec{k}, -\vec{k} \to \vec{k}', -\vec{k}')$ is odd with respect to reversal of the outgoing (or incoming) wave vectors, corresponding to triplet pairing. From Fig. 3(c) it can inferred that the pair partners $(\vec{k}, -\vec{k})$ are on the same SL. The pair scattering between wave vectors near the same Dirac point is attractive, and from one to the other Dirac point it is repulsive. As shown in Fig. 3(d), the zero-total-momentum part of the effective interaction follows closely the form $-V_f d_f(\vec{k}) d_f(\vec{k}')$ with the f-wave form factor $d_f(\vec{k}) = \sin(k_x) - 2\sin(k_x/2) \times \cos(\sqrt{3}k_y/2)$. The pairing has the same sign on the two SLs. The corresponding meanfield picture gives a nodeless state with gap amplitudes of opposite sign on the two Fermi circles. In real space, the pairing with $d_f(\vec{k})$ takes place between a given site and its 6 next-nearest neighbors, with sign change upon a $\pi/3$-rotation around the site. Thus the

pairing is not directly mediated by the nearest-neighbor repulsion V, but due to a next-nearest-neighbor attraction generated by higher orders of V in the FRG flow. Consistently, if we introduce a next-nearest-neighbor attraction $V_2 < 0$, the pairing instability is enhanced. Note that this pairing is quite different from the nearest-neighbor inter-SL pairing found in a mean field study in Ref. [16] for attractive V. In full agreement with the interactions, the flow of the f-wave susceptibility with form factor $d_f(\vec{k})$ [see Fig. 3(a)] shows a strong upturn once the CDW susceptibility is cut off by sufficient doping. Other pairing susceptibilities grow much more weakly.

Doping into the SDW regime for $U > U_c$ does not produce any measurable scale for a superconducting instability within our numerical precision. The SDW regime just gives way to a stable Fermi liquid. The SDW regime can also be generated in the FRG by a nearest-neighbor AF Heisenberg interaction $J > 2t$. Doping into this state [see Fig. 3(b)], the SDW scale drops down. Now, for $J > 2t$, we find an instability in the singlet-pairing channel with d-wave symmetry, confirming the results of a meanfield decoupling of the J-term [17]. The energetically best state is the complex linear combination of the two degenerate basis function d_{xy} and $d_{x^2-y^2}$, leading to a fully gapped time-reversal-symmetry-breaking state [17]. In Fig. 3(d) we show the effective pair scattering. It follows closely the ansatz $-V_d[d^*_{x^2-y^2}(\vec{k})d_{x^2-y^2}(\vec{k}') + d^*_{xy}(\vec{k})d_{xy}(\vec{k}')]$ with the form factors corresponding to the next-nearest-neighbor pairing of $d_{x^2-y^2}$- and d_{xy}-type, $d_{x^2-y^2}(\vec{k}) = e^{-ik_y/\sqrt{3}} - e^{ik_y/(2\sqrt{3})}\cos k_x/2$ and $d_{xy}(\vec{k}) = ie^{ik_y/(2\sqrt{3})}\sin k_x/2$.

Regarding possible realizations of Cooper pairing, we note that a sizable T_c for the triplet-pairing requires dominant nearest-neighbor repulsion $V > U$ large enough to be at least close to a CDW ordered state for zero doping. $V > U$ could be realized due to Holstein phonons, reducing the effective U [26]. A CDW state (or an antiferromagnetic insulator indicative of strong Heisenberg exchange J which could lead to robust $d + id$ pairing), however, does not seem to be realized in graphene. Yet, for graphene on a substrate, there have been theoretical ideas [27] that out-of-plane vibrations of the carbon atoms with opposite amplitude on the two SLs could trigger a CDW instability, at least in a magnetic field. If the system is near such an instability, the phononic fluctuations would add to the intrinsic fluctuations, and move the system closer to the parameter range for triplet pairing. Recent photoemission work [28] for graphene on *SiC* substrates revealed a gap-like feature near the Dirac points, interpreted as AB-SL symmetry-breaking by the substrate. If this gap is in fact a cooperative effect of substrate and electronic interactions, it would seem promising to dope the system out of gapped phase and to search for superconducting correlations.

In conclusion, we have analyzed instabilities of interacting electrons on the honeycomb lattice using a FRG method. The undoped state becomes unstable with respect to spin-density wave and charge-density-wave instabilities, if onsite or nearest-neighbor repulsions exceed critical values. Upon sufficient doping, the CDW instability gives way to a triplet-pairing instability with intrasublattice Cooper pairing of next-nearest neighbors. Doping of a SDW regime with $J > 0$ leads to a singlet-pairing instability in the d-wave channel.

C. H. thanks A. Black-Schaffer, J. N. Fuchs, G. H. Gweon, and M. Kinza for discussions and BaCaTec for support.

[1] K. S. Novoselov *et al.*, Proc. Natl. Acad. Sci. U.S.A. **102**, 10451 (2005).
[2] For a review, see A. K. Geim and K. S. Novoselov, Nat. Mater. **6**, 183 (2007).
[3] C. W. J. Beenakker, Phys. Rev. Lett. **97**, 067007 (2006).
[4] M. I. Katsnelson K. S. Novoselov, and A. K. Geim, Nature Phys. **2**, 620 (2006).
[5] B. Trauzettel *et al.*, Nature Phys. **3**, 192 (2007).
[6] See however A. Bostwick *et al.*, Nature Phys. **3**, 36 (2007).
[7] T. Weller *et al.*, Nature Phys. **1**, 39 (2005); G. Csanyi *et al.*, Nature Phys. **1**, 42 (2005).
[8] Y. Kopelevich, P. Esquinazi, J. Low Temp. Phys. **146**, 629 (2007).
[9] J. Gonzalez, F. Guinea, and M. A. H. Vozmediano, Phys. Rev. Lett. **77**, 3589 (1996); Phys. Rev. B **59**, R2474 (1999).
[10] S. Das Sarma, E. H. Hwang, and W.-K. Tse, Phys. Rev. B **75**, 121406 (2007).
[11] A. H. Castro Neto and F. Guinea, Phys. Rev. B **75**, 045404 (2007).
[12] S. Sorella and E. Tosatti, Europhys. Lett. **19**, 699 (1992).
[13] A. L. Tchougreff and R. Hoffmann, J. Phys. Chem. **96**, 8993 (1992).
[14] D. V. Khveshchenko, Phys. Rev. Lett. **87**, 246802 (2001).
[15] I. F. Herbut, Phys. Rev. Lett. **97**, 146401 (2006).
[16] B. Uchoa and A. H. Castro Neto, Phys. Rev. Lett. **98**, 146801 (2007).
[17] A. M. Black-Schaffer and S. Doniach, Phys. Rev. B **75**, 134512 (2007).
[18] S. Raghu *et al.*, arXiv:0710.0030 [Phys. Rev. Lett. (to be published)]..
[19] D. Zanchi and H. J. Schulz, Europhys. Lett. **44**, 235 (1998).
[20] C. J. Halboth and W. Metzner, Phys. Rev. B **61**, 7364 (2000); Phys. Rev. Lett. **85**, 5162 (2000).
[21] C. Honerkamp *et al.*, Phys. Rev. B **63**, 035109 (2001).
[22] C. Honerkamp and M. Salmhofer, Phys. Rev. B **64**, 184516 (2001); Phys. Rev. Lett. **87**, 187004 (2001).
[23] S. W. Tsai and J. B. Marston, Can. J. Phys. **79**, 1463 (2001).
[24] C. Honerkamp, Phys. Rev. B **68**, 104510 (2003).
[25] M. Salmhofer and C. Honerkamp, Prog. Theor. Phys. **105**, 1 (2001); also R. Shankar, Rev. Mod. Phys. **66**, 129 (1994).
[26] G. Sangiovanni *et al.*, Phys. Rev. Lett. **94**, 026401 (2005).
[27] J.-N. Fuchs and P. Lederer, Phys. Rev. Lett. **98**, 016803 (2007).
[28] S. Y. Zhou, Nat. Mater. **6**, 770 (2007).